Turbulence in wide-angle conical diffusers with swirling flow

H.A. Abdalla, M. M. El-Mayit, A. A. Abd El-Hamid and A. M. El-Shazly
Mechanical Power Eng. Dept., Faculty of Eng., Minoufiya University, Shebin El-Kom, Egypt

Turbulent swirling flow through wide-angle conical diffusers, with inlet swirl intensities sufficient to avoid flow separation are predicted by k-ε Reynolds stress turbulence model. The main objective of this study is developing numerical predictions of the detailed turbulence quantities for swirling diffuser flows, regarding the effect of inlet swirl type. The effects of inlet swirl intensity and inlet swirl profile on the flow characteristics are also discussed. Comparisons between predicted results and published data are performed to verify the mathematical model. A good agreement is obtained with available experimental data for the mean velocities and Reynolds stresses quantities. With swirling flow, the location of the turbulence peak shifts towards the diffuser centerline as the flow proceeds in the downstream direction due to the effect of pressure gradient with swirl. The Solid-Body Rotation (SBR) inlet swirl flow causes a rapid axial velocity decay in the core region than does with the Free-Vortex (FV) inlet swirl flow and increases the near-wall axial velocity which tends to retard near-wall flow separation.

يقدم البحث دراسة نظرية للسريان الإضطرابى الدوامى الغير قابل للإنضغاط خلال النواشر المخروطية ذات زاوية إنفراج كبيرة ولحالة شدة دوامية عند الدخول للناشر كافية لمنع الإنفصال للسريان المحورى. وذلك بإستخدام النموذج الرياضى الذى يحكم السريان فى الإتجاهات الثلاثة (المحورى – القطرى – المماسى) مع إستخدام نموذج الإضطراب k-ε والذى يتضمن الإجهادات الإضطرابية العمودية والمماسية. يهدف هذا البحث إلى دراسة تأثير ونوع الشدة الدوامية عند المدخل للناشر على كيفية تغير طاقة الحركة الإضطرابية والإجهادات الإضطرابية العمودية والمماسية Reynolds stresses والتى تؤثر على خصائص السريان وحدوث الإنفصال فى النواشر المخروطية ذات زاوية إنفراج كبيرة وذلك للحصول على أفضل أداء للنواشر التى تعمل تحت هذه الظروف. تم عمل مقارنة بين النتائج النظرية والنتائج المعملية المتاحة من الأبحاث المنشورة وذلك للتحقق من دقة النموذج الرياضى ، وقد أظهرت الدراسة تقارب جيدا ومقبولا بين النتائج النظرية والمعملية.

Keywords: Conical diffuser, Swirl flow, Turbulence, Separation, Recirculation

1. Introduction

Diffusers are important elements in turbomachinery and are commonly used in many other fluid devices to convert kinetic energy into pressure energy. In flow through a diffuser, the total pressure loss is caused by the wall friction and flow turbulence. The turbulence loss increases with the increase of diffuser divergence angle, and if the rate of divergence is great enough, flow separation at the walls occurs. The total pressure loss is dependent on the geometrical parameters and inlet conditions. Extensive literature on conical diffusers is available, and several reviews have been conducted by many investigators [1 to 5]. It has known that certain types of inlet swirl and inlet distortion increased diffuser pressure recovery coefficients. The swirling inlet velocity component in the diffuser is often observed in flow downstream of the turbomachines or certain types of combustor chambers. The effect of inlet swirl on conical diffuser performance was experimentally studied by McDonald et al. [6] and Senoo et al. [7]. With the swirling velocity component, the flow is less likely to separate even if the divergence angle of diffuser is large, and a high-pressure recovery coefficient is observed. However, excessive amount of swirl results in a low-pressure recovery rate. Moore and Kline [8], Sajben et al. [9], and Hoffmann [10] altered inlet velocity and turbulence characteristics to maintain large effective area for improving the overall efficiency of wide-angle diffusers. The one aspect of diffuser study which has received little attention is the investigation of the turbulence characteristics of the swirling flowfield. In non-swirling flow, an investigation was performed to analyze the

structure of turbulence in conical diffuser [11]. The results showed that, a significant peak in all of the turbulence quantities occurs but displaced from the diffuser wall as the flow proceeds into the diffuser. Unfortunately, a few experimental data for turbulence quantities of swirling flow in conical diffusers have been reported [12, 13]. They measured Reynolds stresses within the boundary layer in the presence of swirl flow in the 20 degrees conical diffuser. The measurements conducted for only swirl intensity of 0.3.

Flow in diffusers present several interesting features such as the presence of regions of separation and recirculating flows, strong streamline curvature and adverse pressure gradient so that turbulent swirling flows in conical diffusers are extremely complicated. A few numerical predictions for turbulence quantities of swirling flows in wide-angle conical diffusers have been reported. Previous numerical predictions have been obtained using algebraic eddy-viscosity models, two-equation turbulence models, and algebraic Reynolds sress models for swirling flow in conical diffusers with and without a tail pipe [14-17]. Okhio et al. [14] predicted the mean velocities in a 16.5 degrees diffuser with a tail pipe using a Prandtl mixing length model. Armfiled and Fletcher [15] predicted mean velocities fields in a 7 degrees diffuser using a reduced form of Navier-Stokes equations with a mixing length turbulence model. Habib and Whitelaw [16] calculated swirling recirculating flows using a k- ε turbulence model in wide-angle diffusers of 40 and 90 degrees with relatively longer tail pipes than the diffuser section. Hah [17] used an algebraic Reynolds stress model to predict the flow characteristics in two diffusers (8 and 16 degrees). Most of previous studies concentrated on the performance of conical diffusers regardless the turbulence structure. In recent years, numerical methods have been extensively developed for the simulation of non-swirling turbulent flow in diffusers. Most of such numerical studies solve the time-averaged Navier-Stokes equations combined with turbulence models and others using the integral method [18-21]. It was pointed out that the predictions for this problem are strongly affected by the level of turbulence intensity, adverse pressure gradient and the approaching flow at the diffuser entrance. Some predictions have shown reasonable agreements with measurements. As the accuracy of physical models and the capacity of computers increase, efforts on numerical simulation of the flow field in the diffusers are being made and must be employing fine mesh for numerical solution of diffuser flows. Authors have previously reported on swirling flow through smooth and rough wide-angle conical diffusers, and concluded that, the inclusion of swirl upstream of the diffuser inlet prevents separation. Increasing the surface roughness makes the swirl decay faster and the diffuser performance is reduced [22]. It is rarely to find predictions of the Reynolds stresses for the practically wide-angle diffusers with total divergence angle ranged from 10-30 degrees [23, 24]. Therefore, the main objective of this study is developing numerical predictions of the detailed turbulence quantities for swirling diffuser flows, regarding the effect of inlet swirl type. This study is very important for understanding the physical aspects of swirling turbulent flow characteristics in the presence of pressure gradient.

2. The mathematical formulation

2.1. Governing equations and turbulence closure modeling

The problem under consideration is governed by the steady two-dimensional axisymmetric form of the continuity and the time-averaged Navier-Stokes equations. The cylindrical coordinate-system (x, r, θ) is used to describe the swirling flow in the axisymmetric conical diffuser, fig. 1. For the present study, the steady state equations for incompressible, axisymmetric, turbulent swirling flow may be written as follows [25, 26]. The equations governing the continuity, momentum and turbulence model in generalized form can be written as follow, where, u, v and w are the axial, radial and tangential velocities, respectively. ϕ is the general dependent variable. x, r, and θ are the axial, radial and tangential coordinates. ρ and Γ_ϕ are the density and the effective diffusivity

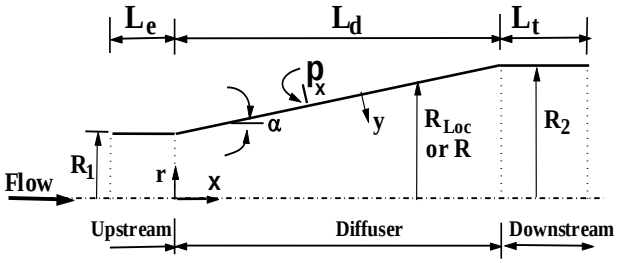

Fig. 1. Diffuser geometrical parameters.

$$\frac{1}{r}\left[\begin{array}{l}\dfrac{\partial}{\partial x}(\rho u r \phi)+\dfrac{\partial}{\partial r}(\rho v r \phi) \\ -\dfrac{\partial}{\partial x}(r\Gamma_\phi \dfrac{\partial \phi}{\partial x})-\dfrac{\partial}{\partial r}(r\Gamma_\phi \dfrac{\partial \phi}{\partial r})\end{array}\right]=S_\phi\,, \tag{1}$$

coefficients. S_ϕ is the source of ϕ. In the present calculations, equations were solved for mean continuity and with dependent variables, ϕ, corresponding to the axial, radial and tangential velocity components. The effective diffusivity was calculated from the two-equations k-ε turbulence model that is valid for both smooth and rough surfaces by incorporating the equivalent sand-grain roughness height into the model functions.

The effective viscosity, μ, and the length scale of turbulence motion, ℓ, are given by the following equations, respectively.

$$\mu = \mu_\ell + \rho C_\mu k^2/\varepsilon\,, \tag{2}$$

$$\ell = C_\mu k^{3/2}/\varepsilon. \tag{3}$$

Where μ_ℓ is the laminar viscosity. The standard k-ε turbulence closure model involves five modeling constants, C_μ = 0.09, C_1 = 1.44, C_2 = 1.92, σ_1 = 1.0 and σ_2 = 1.3. These values are recommended by Launder and Spalding [25] based on extensive examination of turbulent flows.

The Reynolds stress components are given by the following equations, refs. [25, 27].

$$-\rho\overline{u'^2}=\mu\left(\frac{\partial u}{\partial x}\right)-\frac{2}{3}\rho k\,,\quad -\rho\overline{u'v'}=\mu\left(\frac{\partial u}{\partial r}+\frac{\partial v}{\partial x}\right)$$

$$-\rho\overline{v'^2}=2\mu\left(\frac{\partial v}{\partial r}\right)-\frac{2}{3}\rho k\,,\quad -\rho\overline{u'w'}=\mu\frac{\partial w}{\partial x}$$

$$-\rho\overline{w'^2}=2\mu\left(\frac{v}{r}\right)-\frac{2}{3}\rho k\,,\quad -\rho\overline{v'w'}=\mu\left[\,r\frac{\partial}{\partial r}\left(\frac{w}{r}\right)\right], \tag{4}$$

where k is the local value of the turbulent kinetic energy,

$$k=0.5(\overline{u'^2}+\overline{v'^2}+\overline{w'^2}). \tag{5}$$

2.2. Boundary conditions

The governing equations by themselves do not yield a solution to a given problem. Additional boundary information is required at the inlet, outlet, the axis of symmetry and the solid wall. The inlet plane is located for enough upstream the diffuser inlet. Therefore, inlet velocity profiles corresponding to uniform flow were considered at the inlet section. In the case of swirling flows, the tangential velocity profile of a forced vortex was assumed at the inlet section. The inlet conditions required for the turbulence model are the turbulence intensity and the turbulence length scale. These values are set according to refs. [28, 29], the turbulence intensity was taken as 3 % when experimental values were not available, and the characteristic length scale is 0.5 % multiplied by the inlet diffuser diameter. At the exit plane, all of the streamwise gradients of unknown variables were presumed to be constant and overall mass conservation through each cross section was imposed. The exit plane is located far enough downstream where the flow will not influence the upstream properties. Along the axis of symmetry, the gradient in the radial direction of all variables is set to zero, except for the radial velocity component which is given a definite value of zero.

On the solid boundary, the no-slip velocity boundary conditions specified. In the standard k-ε model, viscous diffusion are neglected and empirical wall functions are used to bridge the viscous layer. This is accomplished by relating the velocity component at the first grid node outside this layer to the wall shear stress via the logarithmic law of the wall. A uniform

shear stress prevails in this viscous layer, and generation and dissipation of energy are in balance there via the assumption that the turbulence is in a state of equilibrium. When local equilibrium conditions prevail in the near-wall layer, the near-wall grid node values of k and ε are fixed to the following empirical correlations via the incorporated logarithmic-law option applicable to smooth walls. The wall functions most commonly used are:

$$k_w = u_\tau^2 / \sqrt{C_\mu} \quad ; \quad \varepsilon_w = u_\tau^3 / (\chi\, y) ; \qquad u^+ = \frac{1}{\chi}\, \ell n(Ey^+) \ , \tag{6}$$

where u_τ is the friction velocity, $u_\tau = (\tau_w / \rho)^{0.5}$ and C_μ = 0.09 . χ is the Von-Karman constant, taken to be 0.41, and E is the roughness parameter, taken to be 9.7 for smooth wall.

2.3. Solution procedure

The governing equations were integrated over the two-dimensional axisymmetric control volume which is created by the cylinderical grid system of coordinates to provide the finite difference equations. The discretization scheme used is a hybrid system (an upwind-central difference scheme) explained in detail by Launder and Spalding [25]. The set of the resulting algebraic finite-difference equations were solved numerically by an iterative, line-by-line procedure [26]. A staggered grid system is employed in the present computation. For the grid used in calculations, various grid sizes were used to obtain a grid independent solution. The calculations show that the grid size 53×52 provided grid independent solution. The solution was considered to be converged when the maxima of the mass flux and momentum flux residuals summed at all nodes were less than 0.05 % of the inlet flux.

3. Comparison between the numerical predictions and the measurements

To verify the numerical method, predicted results are compared with existing experimental data for selected flow of conical diffusers. A non-swirling in 8 degrees total divergence angle conical diffuser is predicted and compared with the measured mean and turbulence data of Trupp et al. [30], and Azad and kassab [31] at Re =1.15×10^5. The experimental data of the mean axial and radial velocities and the turbulence quantities, k and $\overline{u'v'}$, are available for comparison at six downstream positions. Others were predicted of the mean axial and radial velocities and the turbulence quantities, [22]. The Reynolds shear stress component $\overline{u'v'}$ is presented in fig. 2-a. Predicted results are very similar except at the first two inlet stations. Near the diffuser entrance, the predicted magnitude of near-wall Reynolds stress component $\overline{u'v'}$ is higher than that the measured values. Singh and Azad [32] extended the measurements of Azad and Kassab [31] for the same conical diffuser configuration. The measurements of Reynolds stress components $\overline{u'^2}$ and $\overline{u'v'}$ are conducted at Re = 0.69×10^5. The predicted and experimental results of turbulent stresses profiles $\overline{u'^2}$ and $\overline{u'v'}$ are shown in fig. 2-b and fig. 2-c. It is seen that the peaks of both profiles of $\overline{u'^2}$ and $\overline{u'v'}$ occur near the diffuser wall and then the peaks are shifted toward the center of the diffuser as the flow proceeds downstream. This occurs due to the presence of an adverse pressure gradient which increases the boundary layer thickness as the flow moves in the downstream direction. The values of $\overline{u'^2}$ and $\overline{u'v'}$ are found to increase along the flow direction. The difference between the predicted and experimental results in the outer region of the conical diffuser may referred to the higher uncertainties in the pulsed-wire measurements in the wall region and small instantaneous back flow in the outer region of the diffuser, as given in [32]. Qualitative agreement of $\overline{u'^2}$ and $\overline{u'v'}$ profiles is also achieved with the experimental data.

The experimental data, on the effect of the swirl by Senoo et al. [7], are used for comparison purpose. They investigated

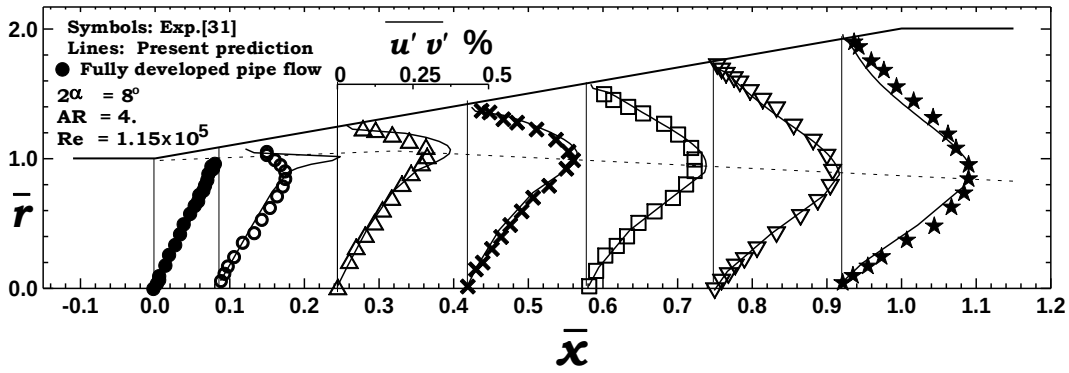

Fig. 2-a. Shear stress ($\overline{u'v'}$).

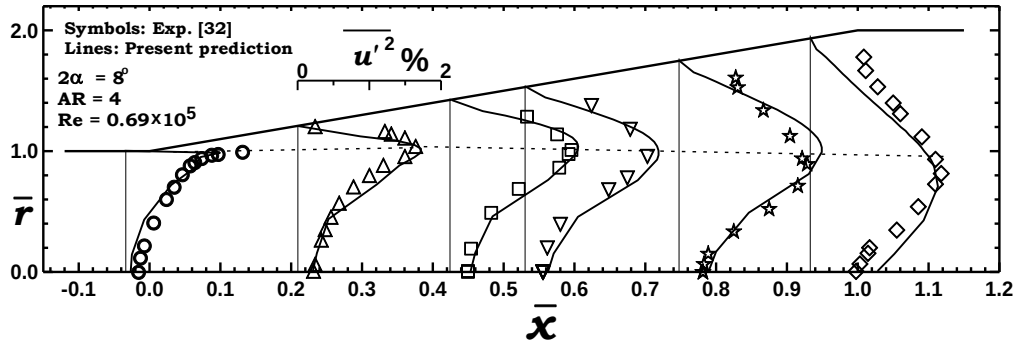

Fig. 2-b. Normal stress ($\overline{u'v'}$).

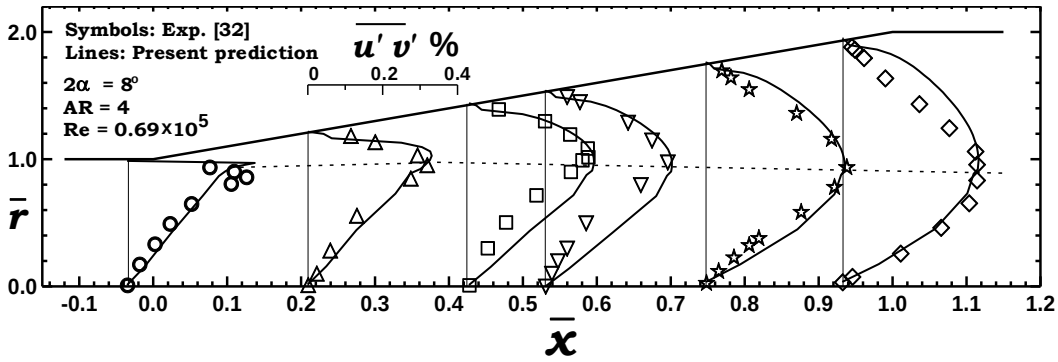

Fig. 2-c. Shear stress ($\overline{u'v'}$).

swirling conical diffuser flow with a FV inlet swirl profile. The tested diffuser has an angle of 16 degrees with an area ratio of 4.0 and flow Reynolds number of 3×10^5. Four different swirl intensities were tested, namely S_1 = 0.0, 0.07, 0.12 and 0.18, and the velocity measurements at the inlet and exit of the diffuser were reported in addition to pressure recovery coefficients. No experimental data for the turbulence quantities are available. The predicted velocity profiles at the outlet of the 16-diffuser and the overall pressure recovery coefficient were compared with the experimental data of Senoo et al. [7]. Fig. 3-a presents a comparison of the axial velocity profile at the diffuser exit for the tested swirl intensities. As seen, for the non-swirling flow condition, predicted values are in good agreement with

swirling conical diffuser flow with a FV inlet swirl profile. The tested diffuser has an angle of 16 degrees with an area ratio of 4.0 and flow Reynolds number of 3×10^5. Four different swirl intensities were tested, namely the experimental data. On the other hand, relatively small disagreement is observed as the swirling intensity is increased. The tangential velocity at the outlet of the 16-diffuser for tested values of swirl intensities is shown in fig. 3-b. Although most of the predictions are adequate, some disagreement is observed at some portions of the diffuser. It is also shown that, the free-vortex inlet swirl profile becomes flattened at the diffuser outlet, and this is predicted very well. The variation of pressure recovery coefficient with swirl intensity is shown in fig. 3-c. The predictions are in good agreement with the experimental data. However, beyond a swirl intensity of approximately 0.1, the computations give values slightly lower than those measured.

Measurements of turbulence quantities for the 20 degrees swirling diffuser flow have been made by Clausen et al. [13]. The inlet swirl type is a Solid-Body Rotation (SBR). Measured profiles of axial and tangential velocity components at the diffuser inlet are used for the

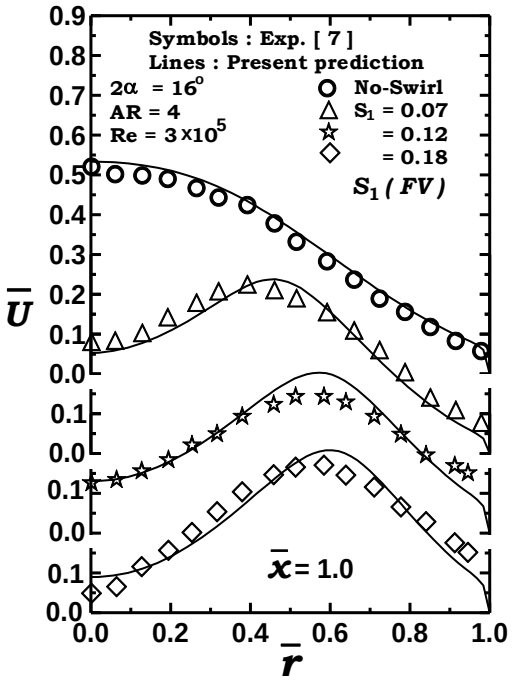

Fig. 3-a. Axial velocity.

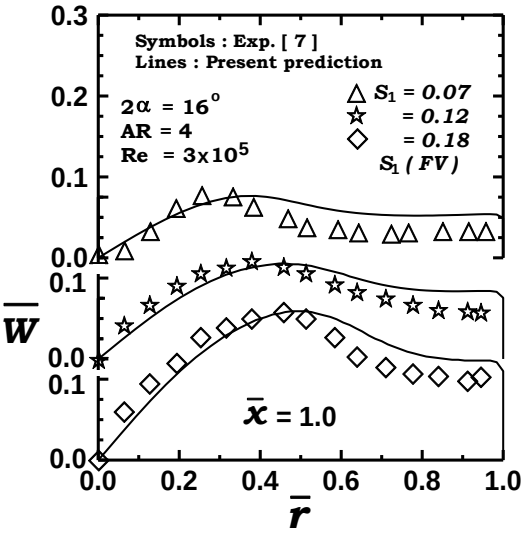

Fig. 3-b. Tangential velocity.

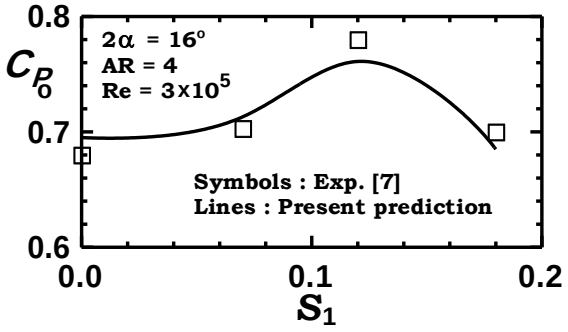

Fig. 3-c. Overall pressure recovery coefficient.

calculations. Fig. 4-a shows a comparison of the experimental data and the prediction for the radial distributions of the axial velocity along the diffuser. It is found from the numerical prediction that, the mathematical model predicts reasonably the effect of swirl in reducing the centerline axial velocity and increasing the near-wall axial velocity. The predicted tangential velocity distributions are presented in fig. 4-b. It can be noted that an excellent agreement all the way to the last station downstream. In the region near to the diffuser exit, however, there is a discrepancy which is due to an initial back flow occurs near the center of the diffuser, for the last two stations. Fig. 4-c shows the radial distributions of the turbulent kinetic energy $\overline{K}$, the

normal Reynolds stress components ($\overline{u'^2}$, $\overline{v'^2}$ and $\overline{w'^2}$) and the tangential shear stress $\overline{u'v'}$ profiles at three locations along the diffuser. The data shown in the figure were normalized by the square of the inlet average velocity at the diffuser inlet. The numerical model predicts reasonably the magnitude and location of the turbulent kinetic energy peak near the wall and the flow characteristics. However, under-predicted values of $\overline{K}$ and $\overline{u'^2}$ downstream of the diffuser entrance are observed. The reason for this behaviour is thought to be referred to the strong variation of adverse pressure gradient at the diffuser inlet and the experimental error.

4. Discussion of predicted results

The diffuser geometry of Clausen et al. [13] is used in the present study. Moreover, a tail pipe is assumed to be fitted at the diffuser outlet in order to investigate the flow characteristics with a separating flow in this diffuser. The prediction of mean flow and turbulence quantities is performed to asses

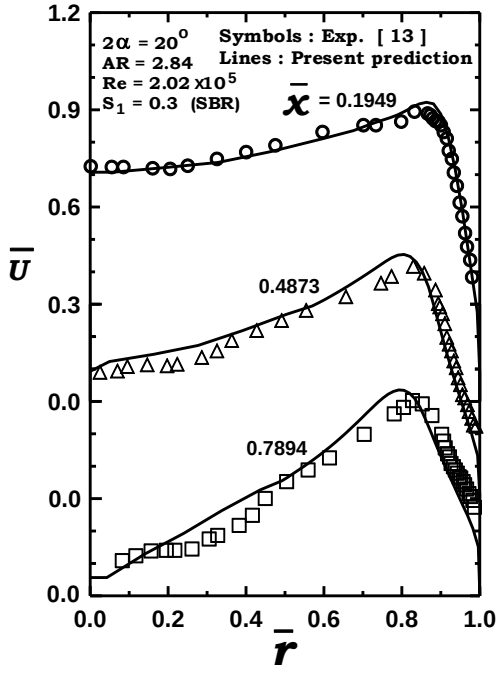

Fig. 4-a. Axial velocity.

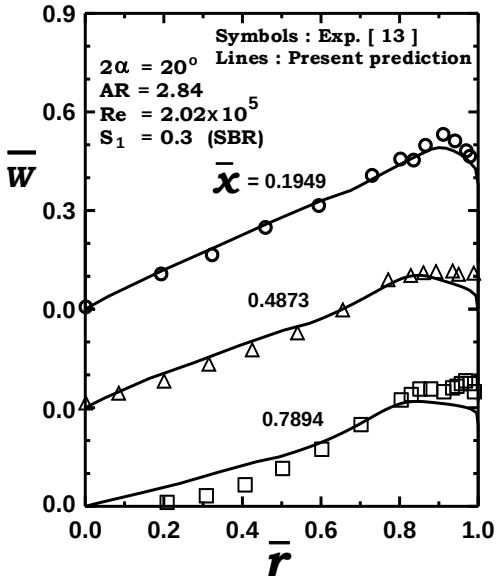

Fig. 4-b. Tangential velocity.

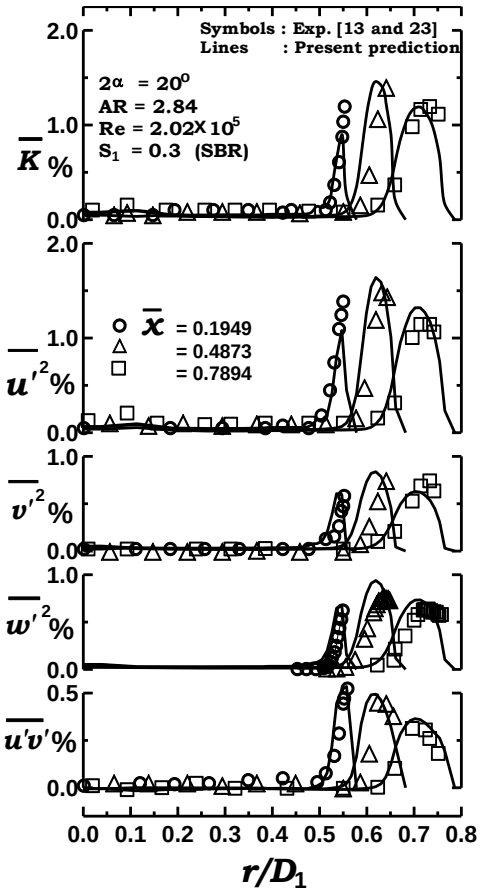

Fig. 4-c. Turbulent kinetic energy and Reynolds stresses.

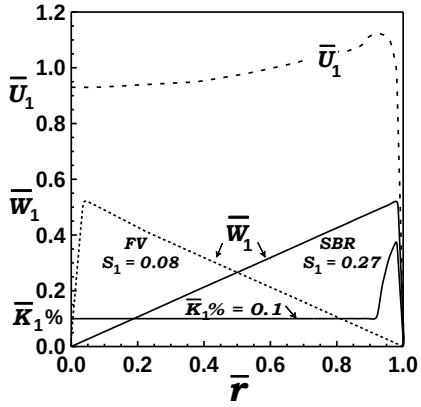

Fig. 5. Inlet conditions for axial velocity , tangential velocity (SBR & FV) and turbulent kinetic energy.

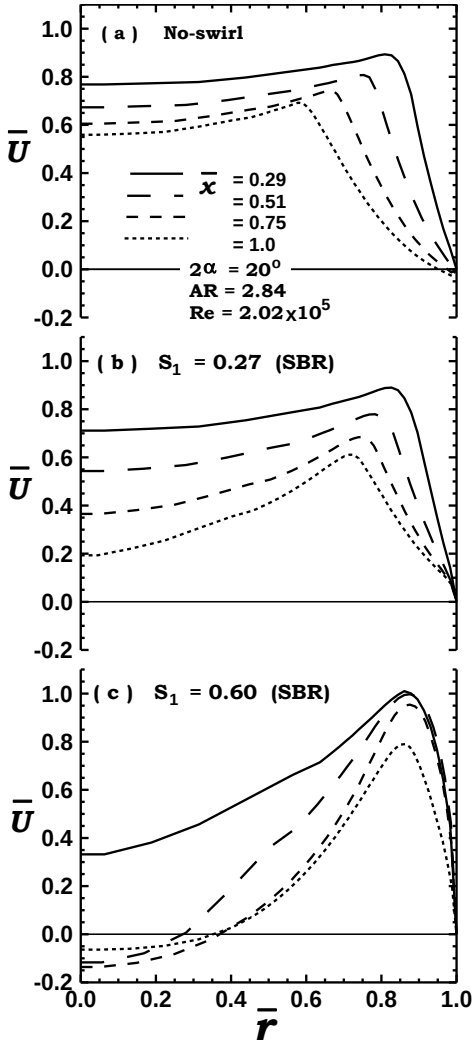

Fig. 6. Predicted axial velocity profiles for non-swirling and swirling flow (SBR) at different downstream sections.

the effects of the inlet swirl intensity and the inlet swirl type on the turbulence characteristics. A SBR inlet swirl profile corresponding to the experimental data of Clausen et al. [13] is predicted and compared with the prediction of a free-vortex inlet swirl flow. The FV inlet velocity profile is taken as a mirror image of the measured solid-body rotation inlet swirl profile [13], as shown in fig. 5.

The predicted axial mean velocities for non-swirling and swirling flows are plotted in fig. 6. The figure indicates that, the decrease in the slope and magnitude of velocity profiles especially near the wall is due to retardation of the fluid flow as a result of the adverse pressure gradient in the downstream direction, fig. 6-a. The results indicate flow separation near to the diffuser exit for non-swirling condition. Fig. 6-b shows that, the inclusion of forced-swirl with intensity of 0.27 at the diffuser inlet suppresses the flow separation and produces much faster decay in the centerline axial velocity than in the non-swirling flow case. But a stronger swirl intensity of 0.6 results in a near-centerline flow recirculation in the diffuser outlet region, fig. 6-c. Fig. 7 shows the tangential velocity distribution at different sections of diffuser. The position of maximum tangential velocity shifts towards the diffuser centerline as the flow proceeds in the downstream direction. The influence of the wall causes a reduction of the tangential velocity. The maximum tangential velocity and the maximum axial velocity as shown in figs. 7-a and 6-b having, approximately, occurs at the same radial position around $\overline{x}$ = 0.51. After this position, the tangential velocity profile flattens out near the wall which leads to an extra production of turbulent energy. However, the strong swirl intensity increases the tangential velocity in the core region near to the diffuser exit due to the formation of a recirculation region which decreases the effective area of pressure rise, fig. 7-b.

Fig. 8 shows the turbulent kinetic energy distribution for non-swirling and swirling flows. The magnitude of $\overline{K}$ is very small in the core region and rises to a maximum value close to the wall, then falling to zero at the wall. For no-swirl flow, the axial variation of the near-wall peak is seen to increase in

magnitude in the downstream direction, fig. 8-a. The location of the turbulence peak shifts towards the diffuser centerline as the flow proceeds in the downstream direction due to the effect of pressure gradient with swirl. In case of moderate swirling flow, fig. 8-b, the magnitude of the turbulent kinetic energy is seen to increase to a maximum at $\bar{x}$ = 0.51. Further downstream, the turbulent kinetic energy peak decays, which is consistent with the experimental data shown in fig. 4-c. It is shown also, the magnitude of turbulent kinetic energy in case of non-swirling flow is higher than that of swirling flow due to the presence of flow separation near to the diffuser outlet. With strong swirl flow, the turbulent kinetic energy rapidly increases in the core region because the recirculation region is enlarged and moves towards the diffuser entrance, fig. 8(c).

Fig. 9 shows the predicted normal radial distributions of the Reynolds stress components ($\overline{u'^2}$, $\overline{v'^2}$ and $\overline{w'^2}$) for non-swirling flow case. It is observed that the peak which is developed close to the wall near the diffuser inlet moves outwards in the streamwise direction. Apparently the level of $\overline{u'^2}$ is higher than those of $\overline{v'^2}$ and $\overline{w'^2}$, as shown in fig. 9-a, 9-b and 9-c, due to the greater contribution of axial velocity gradients to production of turbulent kinetic energy. The Reynolds shear stress component, which is the only shear stress component in a non-swirling axisymmetric case is shown also in fig. 9-d. The peak values of $\overline{u'v'}$ generally increase and the location of the peak moves quickly away from the wall, resulting in the initiation and rapid separation in this region. Generally, the development of peaks with a trend similar to those noted for the normal stresses. The trend is agree with the experimental data of Okwuobi and Azad [11]. It is evident also that, the magnitudes of Reynolds shear stress maxima at various stations increase rapidly in the initial sections and slowly in the final sections of the present diffuser. This behaviour is similar to the growth of the pressure rise along the diffuser.

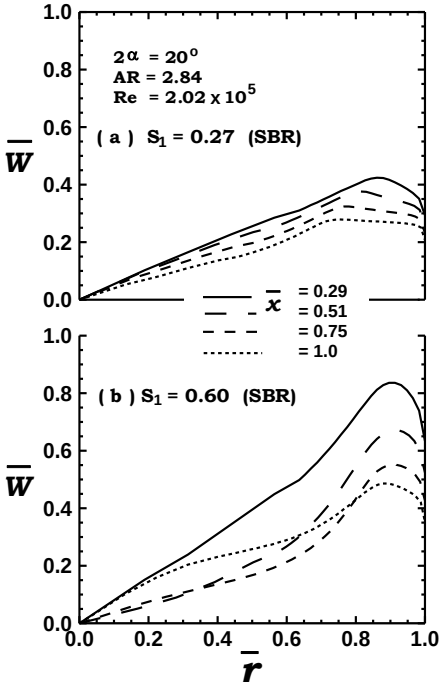

Fig. 7. Predicted tangential velocity profiles for swirling flow (SBR) at different downstream sections.

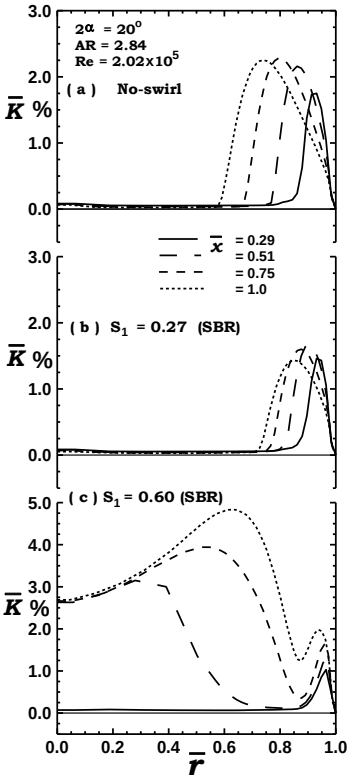

Fig. 8. Predicted Turbulent kinetic energy profiles for non-swirling and swirling flow (SBR) at different downstream sections.

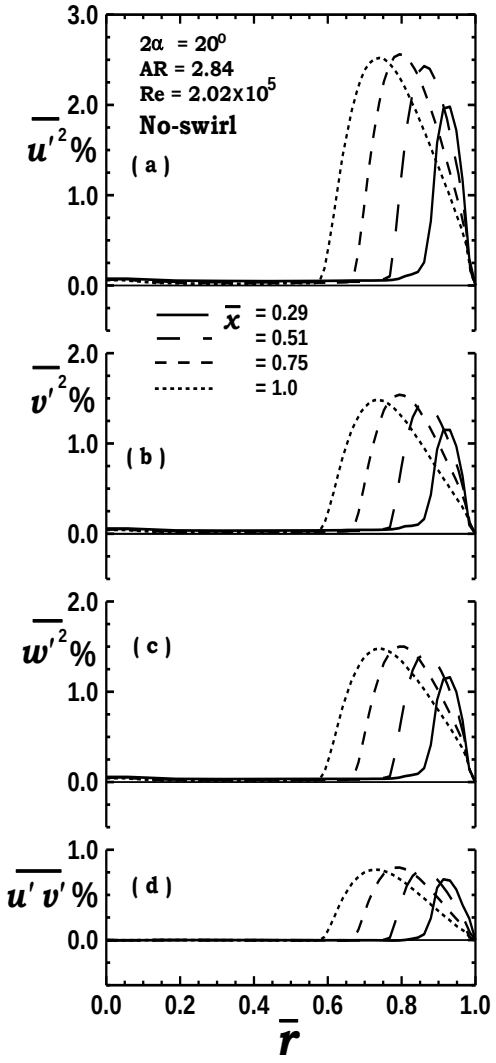

Fig. 9. Predicted Reynolds stresses for non-swirling flow at different downstream sections.

Fig. 10 shows the normal Reynolds stresses components ($\overline{u'^2}$, $\overline{v'^2}$ and $\overline{w'^2}$) for the case of SBR swirling flow, S_1 = 0.27. When this case is compared with the non-swirling flow case presented in fig. 9-a, some important changes are seen in the normal Reynolds stresses profiles. The near-wall peaks of the normal Reynolds stresses decrease in the region of the diffuser inlet and then increase downstream in the flow direction up to $\bar{x}$ = 0.51. Afterwards, the level of the normal Reynolds stresses are decreased in the region of diffuser exit. In addition, inclusion of swirl shifts the peak locations towards the diffuser wall. It is also seen that the $\overline{u'^2}$ profiles have the largest values near-wall peaks. The $\overline{w'^2}$ profiles have, approximately, the same magnitude for $\overline{v'^2}$ along the diffuser. The magnitude of peak reaches its maximum value just after the diffuser inlet, because the flow accelerates within a very short distance from the diffuser inlet and then decelerates under the influence of the adverse pressure gradient. This behaviour of turbulence quantities are referred to the effect of radial pressure gradient in the earlier stations caused by the presence of swirl, which may alter the turbulence field in the diffuser. As shown in fig. 11, it is seen from the distributions of pressure gradient along the diffuser wall and its axis that the pressure gradients near to the diffuser inlet are rapidly changed. Whereas, the flow near the axis is subjected to a continuous process of deceleration while the flow in the near-wall diffuser initially accelerates until the readjustment of the pressure distribution is completed shortly after the diffuser inlet, $\bar{x}$ = 0.25. It is found that the inclusion of SBR inlet swirl may not alter the near-wall axial pressure gradient, but the overall shape is not much changed from the non-swirling case. Correspondingly, the peak-positions of the normal Reynolds stresses move away from diffuser wall as the flow is retarded by the axial pressure gradient. Fig. 12 shows the predicted shear stress components of the Reynolds stresses ($\overline{u'v'}$, $\overline{v'w'}$ and $\overline{u'w'}$) for swirling flow in the 20 degrees diffuser with a tail pipe. Predicted results show that the peak levels of $\overline{u'v'}$ in the diffuser inlet region are reduced compared with those of non-swirling flow, fig. 9-d, due to the increase of pressure gradient intensity in the core region with swirling flow, as shown in fig. 11. The peak levels of $\overline{v'w'}$ and $\overline{v'w'}$ are found smaller than that of $\overline{u'v'}$ because the angular momentum decreases along the radius of curvature near the wall. In addition, the reduction may be due to the localized stabilizing effect of convex curvature caused by the diffuser corner at the entrance, [23].

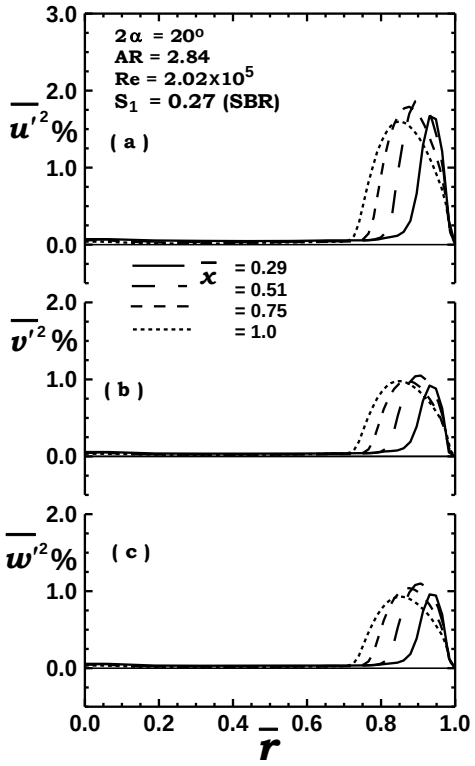

Fig. 10. Predicted normal stresses for swirling flow (SBR) at different downstream sections.

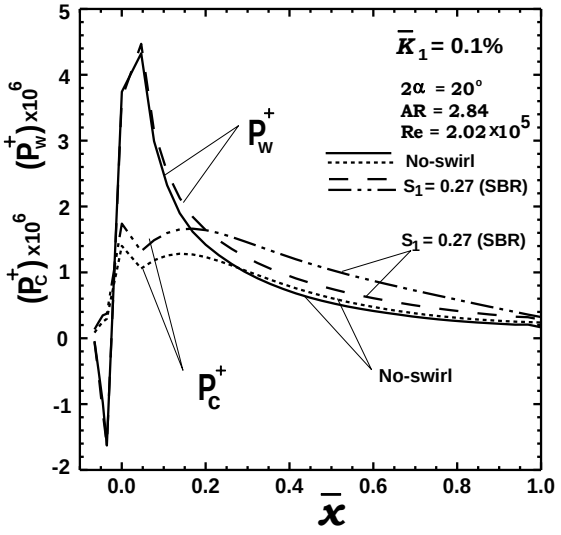

Fig. 11. Predicted pressure gradient along the wall and the core for non-swirling flow and swirling flow (SBR) in conical diffuser.

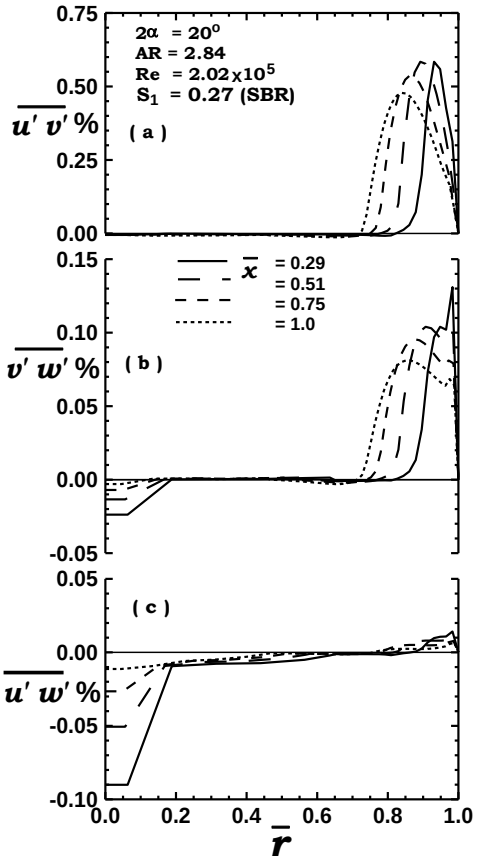

Fig. 12. Predicted shear stresses for swirling flow (SBR) at different downstream sections.

To evaluate the effect of inlet swirl type on the flow characteristics in wide-angle conical diffuser, the flow was also computed with the same inlet conditions of u, v, and k profiles as those for the solid-body rotation swirling and non-swirling flows. The free-vortex inlet swirl profile is taken as a mirror image of the SBR inlet swirl profiles, fig. 5. The outer part of the tangential velocity profile is a free-vortex pattern with the smaller inner part of SBR swirl pattern. Fig. 13 shows the axial and tangential velocity profiles at the diffuser exit for non-swirling and swirling flow with different inlet swirl distributions, for comparison purpose. The SBR swirl causes a rapid axial velocity decay in the core region than those obtained for FV inlet swirling flow and increases the near-wall axial velocity which tends to retard near-wall flow separation, fig. 13-a. The inlet FV swirl profile becomes

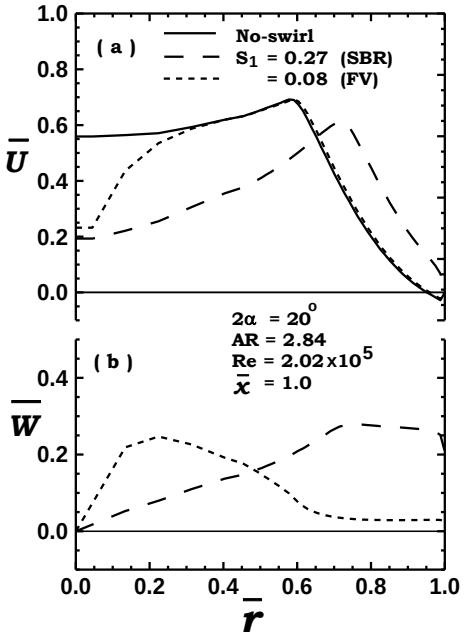

Fig. 13. Predicted axial and tangential velocity profiles at the diffuser exit.

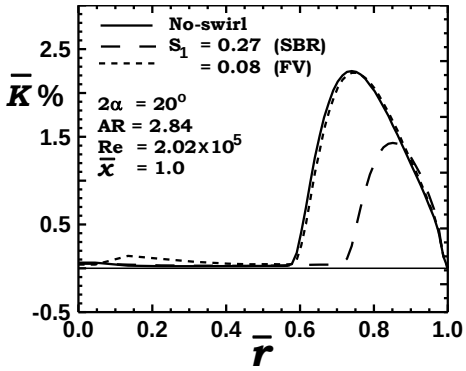

Fig. 14. Predicted turbulent kinetic energy for non-swirling and swirling low at diffuser exit.

flattened at diffuser exit while the SBR swirl profile maintains its general form in the downstream direction, fig. 13-b. Fig. 14 indicates the radial turbulent kinetic energy distributions for the same cases. The most noticeable difference between the SBR swirling flow and the others appears in the near-wall region. The peaks of turbulent kinetic energy for the FV inlet swirling flow and non-swirling flow at the diffuser exit are maintained at approximately the same level and location. It can be concluded that, the inclusion of FV swirl changes the turbulent kinetic energy in the near-wall region slightly little while SBR s

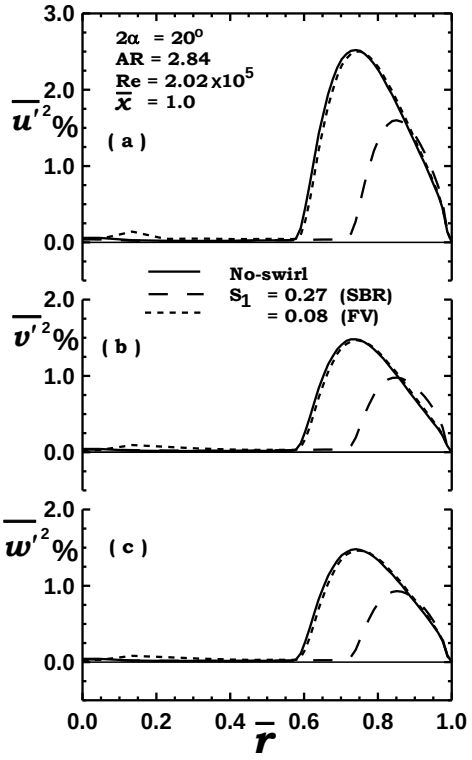

Fig. 15. Predicted normal stresses for non-swirling and swirling flow at diffuser exit.

wirling flow is having a large effect on the turbulence structure in this region. The presence of SBR swirling flow is significantly acting to damp the turbulence in the near-wall region. In addition, the FV swirling flow gives larger values of the turbulence level in the core region than the non-swirling flow because of larger gradients of mean axial velocity components. This means a significant production rate of turbulent kinetic energy is obtained. As expected, the normal stresses $\overline{u'^2}$, $\overline{v'^2}$ and $\overline{w'^2}$ for both cases of swirling flows follow the same behaviour of the turbulent kinetic energy, as shown in fig. 15. Fig. 16 shows the shear stress components ($\overline{u'v'}$, $\overline{v'w'}$ and $\overline{v'w'}$) at the diffuser exit for the three cases tested. The peak levels of $\overline{u'v'}$ for non-swirling and FV inlet swirl have the same behaviour of the normal Reynolds stresses. However, the maximum $\overline{u'v'}$ of non-swirling and FV swirl are larger than that of

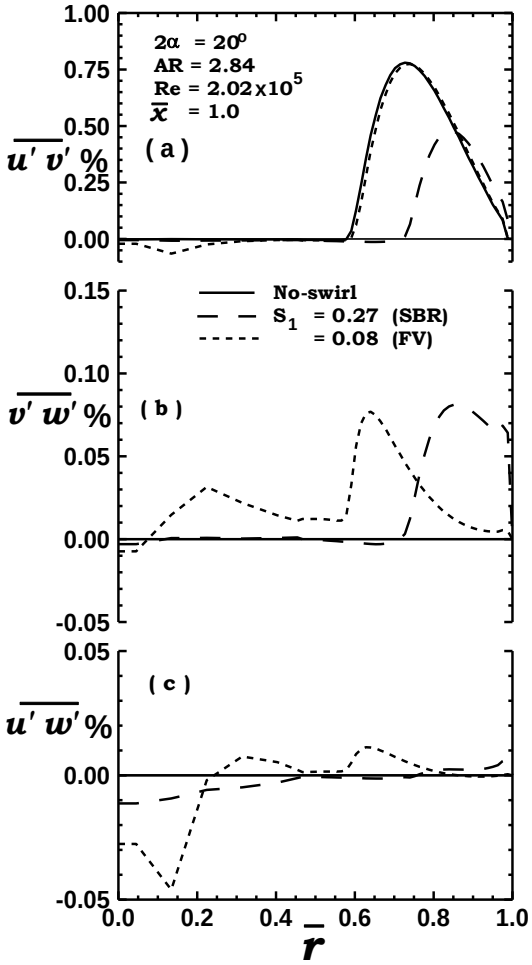

Fig. 16. Predicted shear stresses components of Reynolds stresses at diffuser exit.

SBR swirl case, due to the large gradients of axial and tangential velocities in the near-wall region and the presence of separation flow. The location of the maximum $\overline{u'v'}$ is nearer to the wall than the others because the boundary layer thickness in the presence of SBR swirl is smaller than that of the non-swirling and FV swirl cases. The remarkable observation shown from the distributions of $\overline{v'w'}$ and $\overline{v'w'}$ is the increase of the levels of the shear stresses in core region with the FV swirl. This is referred to the severe negative gradient of FV tangential velocity in the core region and the presence of separation near to the diffuser exit.

5. Conclusions

The main conclusions drawn from the present study are:

1. Good prediction of the mean flow characteristics and turbulence stresses in swirling diffuser flows is obtained.
2. For no-swirl flow, the axial variation of the turbulent kinetic energy, normal and shear stresses increases in the downstream direction and the location of the peak moves away from the diffuser wall.
3. With swirling flow, the location of the turbulence peak shifts towards the diffuser centerline as the flow proceeds in the down-stream direction due to the effect of pressure gradient with swirl. The magnitude of turbulent kinetic energy in the case of non-swirling flow is higher than that of swirling flow due to the presence of wall separation. With strong swirling flow the turbulent kinetic energy rapidly increases in the core region due to the formation of recirculation zone that has a larger size near to the diffuser exit.
4. It is found that the inclusion of SBR inlet swirl may not alter the near-wall axial pressure gradient, but the overall trend is not much changed from the non-swirling case. Correspondingly, the peak-positions of the normal Reynolds stresses move away from the diffuser wall as the flow is retarded by the axial pressure gradient
5. With non-swirling flow, the magnitudes of Reynolds shear stress maxima ($\overline{u'v'}$) at various stations increase rapidly in the initial sections and slowly in the final sections of the wide-angle diffuser, similar to the growth of the pressure rise along the diffuser. The peak values of $\overline{u'v'}$ of non-swirling and FV swirl are larger than that of SBR swirl case, due to the large gradients of axial and tangential velocities in the near-wall region and the presence of separation flow.
6. The inlet SBR swirl causes a rapid axial velocity decay in the core region than does with the FV inlet swirl flow. The near-wall axial velocity increases and the tendency of flow separation is retarded. The inclusion of FV swirling flow gives larger values of the turbulence level in the core region than occurring in the non-swirling flow because of larger gradients of mean axial velocities.

Nomenclature

A is the cross-sectional area, (m^2),
AR is the diffuser area ratio, (A_2 / A_1),
C_p is the local pressure recovery coefficient,
C_p is the $(p_x - p_1)/(\frac{1}{2}\rho U_1^2)$,
C_{Po} is the overall pressure recovery coefficient,
C_{po} is the $(p_2 - p_1)/(\frac{1}{2}\rho U_1^2)$,
D is the diffuser inlet diameter, (m),
E is the roughness parameter eq. (6),
FV is the free-vortex inlet swirl,
k is the turbulent kinetic energy, (m^2/sec^2),
$\overline{K}$ is the dimensionless value of turbulent kinetic energy, $\overline{K} = k / U_1^2$,
L_d is the diffuser axial length, (m),
L_e is the entry pipe length, (m),
L_t is the tail pipe length, (m),
P is the static pressure, (N / m^2),
P^+ is the dimensionless static pressure gradient, $(\frac{\nu}{\rho U_1^3}\frac{dp}{dx})$,
R is the local diffuser radius, (m),
Re is the Reynolds number, $\rho U_1 D / \mu$,
$\bar{r}$ is the dimensionless radial distance, (r/R),
S is the swirl intensity,

$$S = \left(\int_0^R u\, w\, r^2\, dr\right) / \left(R \int_0^R u^2\, r\, dr\right),$$

SBR is the solid-body rotation inlet swirl,
U_1 is the mean-bulk longitudinal velocity, (m/sec),
u, v, w are the local mean velocity in axial, radial and tangential coordinates, (m/sec),
$\overline{U}$ are the dimensionless axial velocity, (u / U_1)
$\overline{W}$ is the dimensionless tangential velocity, (w / U_1),
x, r, θ are the axial , radial and tangential coordinates, m,
$\bar{x}$ is the dimensionless axial distance (x / L_d),
$\overline{u'v'}, w'$ are the velocity fluctuation, components in x, r and θ direction,
$\overline{u'^2}\ \overline{v'^2}$, $\overline{w'^2}$ are the normal stress components in x, r and θ direction, and
$\overline{u'v'}\ \overline{u'w'}$, $\overline{u'w'}$ are the tangential sheer stress components.

Greek symbols

α is the diffuser half-cone angle, (degrees),
ε is the dissipation rate of turbulence kinetic energy, (m^2 / sec^3),
ρ is the density, (k_g / m^3),
μ is the effective viscosity, and ($N.sec/m^2$), and
ν is the kinematic viscosity (m^2 / sec).

Subscripts

1 is the inlet / reference condition,
2 is the diffuser exit condition,
C is the centerline condition,
w is the wall condition, and
x is the axial distance.

Superscripts
— dimensionless and average conditions

References

[1] D.J. Cockrell, and E. Markland, "A Review of Incompressible Diffuser Flow", Aircraft Engineering, Vol. 35 (10), pp. 286-292. (1963). See also: "Diffuser Behavior, A Review of past Experimental Work Relevant Today", Aircraft Engineering, Vol. 46 (1), pp. 16-26 (1974).
[2] A.T. McDonald, R.W. Fox, "Incompressible Flow in Conical Diffusers", Purdue Res. Foundation, TR-1 (1964).
[3] G. Sovran and E.D. Klomp, "Experimental Determined Optimum Geometries for Rectilinear Diffusers with Rectangular, Conical or Annular

Cross-Section", Fluid Mechanics of Internal Flow edited by G. Sovran, Elsevier, Amsterdam, pp. 270-319 (1967).

[4] M. Sajben, J.C. Kroutil, and A.V., Sedrick, "Conical Diffuser Flows with Natural and Screen-Simulated Inlet Conditions", AIAA Journal, Vol. 14 (12), pp. 1723-1730 (1976).

[5] A. Klein, "Review: Effects of Inlet Conditions on Conical-Diffuser Performance", Transactions of The ASME, Journal of Fluids Engineering, Vol. 103, pp. 250-257 (1981).

[6] A.T. McDonald, R.W. Fox, and R.V. Van Dewoestine, "Effects of Swirling Inlet Flow on Pressure Recovery in Conical Diffusers", AIAA Journal, Vol. 9, pp. 2014-2018 (1971).

[7] Y. Senoo, N. Kawaguchi and T. Nagata, "Swirl Flow in Conical Diffusers", Bulletin of the JSME Journal, Vol. 21, (151), pp. 112-119 (1978).

[8] C.A. Moore and S.J. Kline, "Some Effects of Vanes and of Turbulence in Two-Dimensional Wide-Angle Subsonic Diffusers", NACA TN 4080 (1958).

[9] M. Sajben, C.P. Chen, and J.C. Kroutel, "A New Passive Boundary Layer Control Device", Journal of Aircraft, Vol. 14, pp. 654-660 (1976).

[10] J.A. Hoffmann, "Effects of Free-Stream Turbulence on Diffuser Performance", Trans. ASME, Journal of Fluids Engineering, Vol. 103, pp. 385-390 (1981).

[11] P.A.C. Okwuobi and R.S. Azd, "Turbulence in a Conical Diffuser with Fully Developed Flow at Entry", Journal of Fluid Mech. Vol. 57, Part 3, pp. 603-622 (1973).

[12] P.D. Clausen, and D.H. Wood, "Some Measurements of Turbulent Swirling Flow Through an Exisymmetric Diffuser", Proceeding of Sixth Symposium on Turbulent Shear Flows, Edited by F.J. Durst et al., Paul Sabatier Univ., Toulouse, France, Sept. 7-9, pp. 1.3.1-1.3.5 (1987).

[13] P.D. Clausen, S.G. Koh, and D.H. Wood, "Measurements of a Swirling Turbulent Boundary Layer Developing in a Conical Diffuser", Experimental Thermal and Fluid Science Journal, pp. 39 – 48 (1993).

[14] C.B. Okhio, H.P. Horton, and G. Langer,, "Calculation of Turbulent Swirling Flow Through Wide Angle Conical Diffusers and The Associated Dissipative Losses", Int. Journal Heat Fluid Flow, Vol. 7 (1), pp. 37- 48 (1986).

[15] S.W. Armfield, and C.A.J., Fletcher, "Numerical Simulation of Swirling Flow in Diffusers", International Journal for Numerical Methods in Fluids, Vol. 6, pp. 541 – 556 (1986).

[16] M.A. Habib, and J.H. Whitelaw, "The Calculation of Turbulent Flow in Wide Angle Diffusers", Numerical Heat Transfer, Vol. 5 (2), pp. 145- 164 (1982).

[17] C. Hah, "Calculation of Various Diffuser Flows with Inlet Swirl and Inlet Distortion Effects", AIAA Journal Vol. 21 (8), pp. 1127-1133 (1983).

[18] G. Iaccarino, "Prediction of the Turbulent Flow in A Diffuser With Commercial CFD Codes", Center for Turbulence Research, Annual Research Briefs, pp. 271-278 (2000).

[19] M. Vujičić, and C. Crnojević, "Calculation of the Turbulent Flow in a Plane Diffuser by Using the Integral Method", FME Transactions, Vol. 31 (2), pp. 69-74 (2003).

[20] E.J. Braga, and M.J.S., De lemos, "Numerical Simulation of Turbulent Flow in Small-Angle Diffusers and Contractions Using a New Wall Treatment and A Linear High Reynolds k- ε Model", Taylor & Francis Group, Numerical Heat Transfer, Part A, 45,, pp. 911-933 (2004).

[21] J.U. Schlüter, X. Wu and H. Pitsch, "Large-Eddy Simulations of a Separated Plane Diffuser", 43rd AIAA Aerospace Sciences Meeting and Exhibit, January 10-13, /Reno, NV, pp. 1-13 (2005).

[22] H.A. Abdalla, M.M. El-Mayit, A.A. Abd El-Hamid, and A.M. El-Shazly, "Prediction of Swirling Flow and Performance in Smooth and Rough

Wide-Angle Conical Diffusers", Engineering Research Journal, Faculty of Engineering, Minoufiya University, Egypt, Vol. 27 (4), pp. 315-332 (2004).

[23] W.A. Steven, Nam-Hyo Cho and A.J. Clive, "Prediction of Turbulence Quantities for Swirling Flow in Conical Diffusers", AIAA Journal, Vol. 28 (3), March, pp. 453– 460 (1990).

[24] S. Čantrak, M. Benišek, and M. Nedeljković, "Contemporary Problems in Turbulent Swirling Flows", The Scientific Journal FACTA UNIVERSITATIS, Series: Mechanics, Automatic Control and Robotics, UNIVERSITY OF NIŠ, Vol. 2 (7/2), pp. 369-380 (1997).

[25] B.E. Launder, and D.B. Spalding, "The Numerical Computation of Turbulent Flows", Computer Methods in Applied Mechanics and Engineering, Vol. 3, pp. 269-289 (1974).

[26] A.D. Gosman, and W.M. Pun, "Calculation of Re-circulating Flows", Rept. No. HTS/74/12, Dept. of Mech. Engg., Imperial College London, England (1974).

[27] P. Bartsch, N. Weiser, and W. Nitsche, "Numerical Calculations of Variable-Angle Diffuser Flows", Computers and Experiments in Fluid Flow, Editors G.M. Cartomagno and C.A. Brebbia Proceedings of the Fourth International Conference on Computational Methods and Experimental Measurements, Capri, pp. 251– 263 (1990).

[28] D.G. Lillely, and D.L. Rhode, "A Computer Code for swirling Turbulent Combustor Geometries", NASA Contractor, Report 3442 (1982).

[29] F. Pourahamdi, and J.A.C., Humphrey, "Prediction of Curved Channel Flow With an Extended k-ε Model of Turbulence", AIAA J., Vol. 21, pp. 1365-1373 (1983).

[30] A.C. Trupp, R.S. Azad, and S.Z. Kassab, "Near-Wall Velocity Distributions Within a Straight Conical Diffuser", Experiments in Fluids 4, pp. 319-331 (1986).

[31] R.S. Azad, and S.Z. Kassab, "Turbulent Flow in a Conical Diffuser: Overview and Implications", Phys. Fluids A, Vol. 1 (3), pp. 564-573 (1989).

[32] R.K. Singh and R.S. Azad, "Structure of Turbulence in an Incipient-Separating Axisymmetric Flow", Transactions of ASME, Journal of Fluid Engineering, Vol. 117, pp. 338-433 (1995).

Received March 1, 2005
Accepted June 15, 2005